

Chapter 6

Application of Nanoseparation in Reaction Mechanism Analysis



Zhao Cai, Xiaohan Qi, Yun Kuang and Qian Zhang

Abstract Density gradient centrifugation has been established to obtain monodisperse nanoparticles with strictly uniform size and morphology, which are usually hard to be obtained by synthetic optimization. Previous chapters have demonstrated the versatility and universality of such separation method, by which nearly all kinds of nanostructures can be separated, including particles, clusters, and assemblies. Further, reaction mechanism, as well as structure–property relationship, can also be investigated based on the separated fractions. The focus of this chapter is the reaction mechanism analysis using density gradient centrifugation, namely by introducing a distinctive functional gradient layer, such as reaction zone and assembly zone, reaction mechanisms can be therefore studied since the reaction time can be pre-designed and the reaction environment can be switched extremely fast in a centrifugal force field. In a word, “lab in a tube” based on nanoseparation opens a new door for the investigation of synthetic optimization, assembly behavior, and surface reaction of various nanostructures.

Keywords Lab in a tube · Reaction zone · Assembly zone · Growth mechanism
Ultraconcentration

6.1 The Concept of “lab in a tube”

The concept of “lab in a tube” was first put forward as a micrototal analysis system in the field of biology [1, 2]. In recent decades, in order to extend the functionality of old lab-on-a-chip system [3], lab in a tube has been designed to compress an entire laboratory into a smaller architecture, in which lots of individual detection or analysis components were integrated and each could be used individually or together [1].

In 2012, Sun’s group [4] extended this concept to the field of nanoseparation. “lab in a tube” based on nanoseparation is the integration of numerous functional gradient layers into a single centrifuge tube constituting a microsystem of several independent units, each can individually perform its specific role such as “reaction zone” or “assembly zone” (Fig. 6.1).



Fig. 6.1 Schematic cartoon of “lab in a tube” system based on nanoseparation

Since “lab in a tube” system can combine several functionalities such as separating and assembling nanostructures, it can be applied to various research settings. First of all, by introducing a separation zone, nanoparticles with strictly uniform size can be obtained, and their size–property relationship can be therefore investigated. Second, by analyzing the chemical composition or crystal structure of separated fractions, key pieces of information can be obtained to guide synthetic optimization, which are usually difficult to be got by traditional contrast experiments. Third, by introducing a reaction zone, the corresponding reaction mechanism can be investigated since the reaction time can be finely controlled and the chemical environment can be changed soon. Last but not the least, by introducing an assembly zone, the symmetrical or asymmetric assembly of various nanostructures can also be achieved since their directional movement can be specially designed.

6.2 Size–Property Investigation Through DGUC Nanoseparation

Strictly monodisperse nanoparticles with focused size distribution can be obtained through DGUC nanoseparation, which are usually hard to be got by optimized synthesis and can lay a perfect foundation for their size–property investigation. What is more, even the most advanced synthesis technology cannot meet the high standard for fabrication of monodisperse nanostructures with specific parameters,

like ultrashort single-walled carbon nanotubes, DGUC nanoseparation can be used instead to verify theoretical predictions about such nanostructures.

Single-walled carbon nanotubes (SWCNTs) have been extensively studied due to their unique physical and chemical properties, such as the length-dependent optical performance [5–7]. It has been predicted theoretically that the bandgap of a nanotube increases with the length decreasing and quantum confinement effect should be observed as the SWCNTs approach zero-dimensional sizes. However, it is still impossible to obtain monodisperse zero-dimensional SWCNTs by synthetic optimization.

In this case, DGUC nanoseparation can show unique advantages over conventional synthesis methods. As reported by Dai's group in 2008, to obtain ultrashort SWCNTs, low-density gradient layers should be utilized so that the sedimentation velocity of individual SWCNT can be well controlled [8]. As a result, a three-layer step gradient made from 5, 7.5, and 10% iodixanol solutions was used. In addition, the centrifugation time should be accurately controlled at the same time, since insufficient time would lead to an uncompleted separation meanwhile a too-long centrifugation time would cause the sedimentation of all SWCNTs to the bottom of centrifuge tube. After a 3 h centrifugation at a ultrahigh speed (~ 300 kg), SWCNTs 2–50 nm in length could be separated according to their length. As shown in Fig. 6.2, the SWCNTs in fraction 6 were ~ 7.5 nm in length, and the average length of subsequent fractions (f8, f12, and f18) increased gradually to ~ 11 , 27, and 58 nm, respectively. Besides, the corresponding length histograms of the fractions further confirmed the successful separation.

The optical characterization results are shown in Fig. 6.3, in which a clearly continuous and monotonic blueshift can be observed for shorter SWCNT fractions. As to the ultrashort SWCNTs fractions, their UV-Vis-NIR absorption and PL peaks blueshifted up to ~ 30 meV compared to that of longer SWCNTs fractions, which should be attributed to quantum confinement effects.

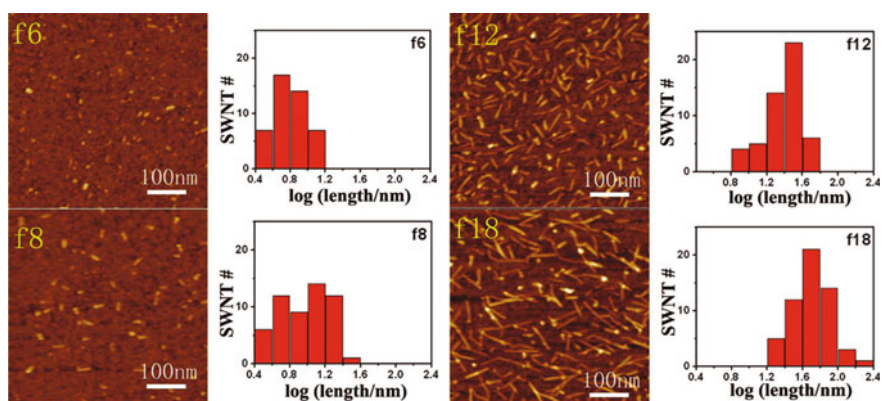


Fig. 6.2 AFM images of SWCNTs in various fractions after separation and the corresponding length histograms of the fractions are shown in the right. Ultrashort SWCNTs (~ 7.5 nm) have been obtained in fraction 6

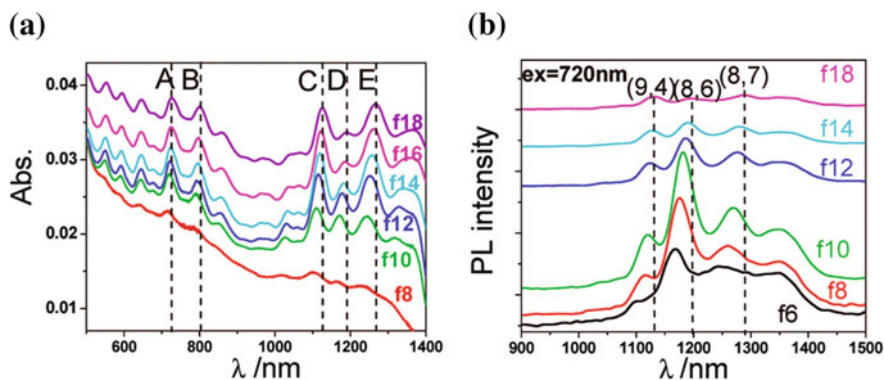


Fig. 6.3 **a** UV-Vis-NIR absorption spectra and **b** NIR-PL spectrum of SWCNTs in various fractions after separation. Blueshift of the absorption peak could be observed in both spectra for shorter SWCNTs

As another example, cadmium selenide nanoparticles (CdSe NPs) are also well-known for their size-dependent fluorescence; even slight difference in size (i.e. 1 nm) could have a significant impact on their fluorescent properties [9]. The DGUC separation of CdSe NPs can therefore pave a new way for their size-property investigation.

In 2010, Sun's group [10] performed the separation in organic density gradients (cyclohexane + tetrachloromethane) as the CdSe NPs were prepared in organic phase. After DGUC separation at 50000 rpm for 60 min, as shown in Fig. 6.4a, the centrifuge tube under UV irradiation at 365 nm showed different colors of

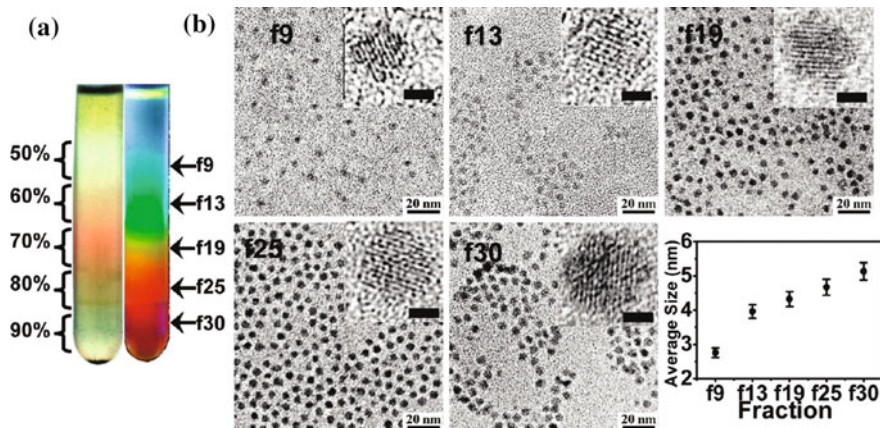


Fig. 6.4 **a** Digital camera images of ultracentrifuge tubes containing CdSe NPs using an organic gradient after size separation. The left one was recorded under natural light and the right one was recorded under ultraviolet light of 365 nm. **b** HRTEM images of corresponding CdSe particle fractions. The inset presents the magnified representative nanoparticle (the bars: 2 nm) and the size evolution of nanoparticles is shown in the bottom right corner

fluorescence, which gave direct evidence to the size separation since larger nanoparticles with more redshifted emissions could be observed at lower gradient layer. The HRTEM images in Fig. 6.4b further confirmed the successful size separation of CdSe NPs.

As the introduction of polystyrene (PS) into organic gradient layers can significantly increase their viscosity, it should slow down the sedimentation of nanoparticles. As expected, PS-containing gradient (vessel II) showed a limited separation compared to PS-free gradient (vessel I) and only applying longer centrifugation time can the separation be completed (vessel III), and thus a finer separation can be achieved. The fluorescence spectra are shown in Fig. 6.5b and c both demonstrated a clear redshift, suggesting the size evolution. It is also worth noting that the discrimination effect was lost in the last few fractions in PS-free gradients, which in turn indicated a finer separation in PS-containing gradient.

In addition, the introduction of polymer makes it possible to fabricate composite films with the separated CdSe NPs after the volatilization of cyclohexane and tetrachloromethane (Fig. 6.5d). Such highly flexible and transparent films could have great potential applications in various fields, such as labeling and information technology.

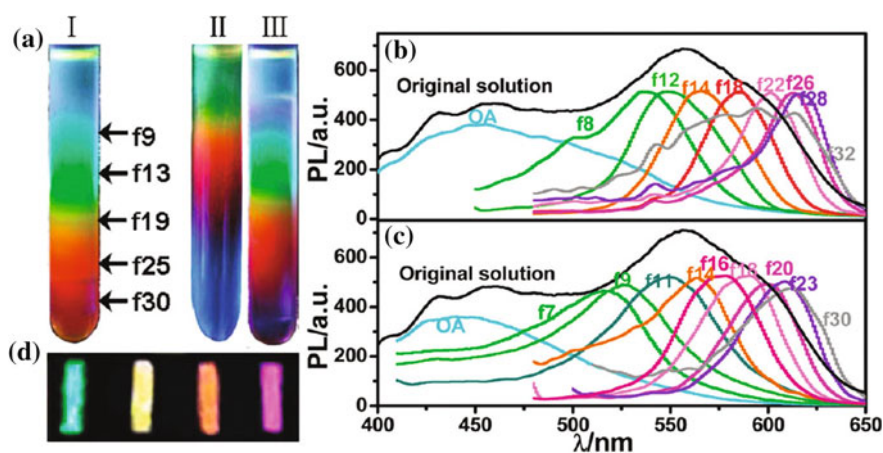


Fig. 6.5 **a** Digital camera images of ultracentrifuge tubes containing CdSe NPs after size separation, recorded under UV irradiation at 365 nm: (vessel I) PS-free gradient, at 50000 rpm for 60 min centrifugation; (vessel II) PS-containing gradient, at 50000 rpm for 60 min centrifugation and (vessel III) PS-containing gradient, at 50000 rpm for 110 min centrifugation. **b** Fluorescence spectra of fractions from vessel I. **c** Fluorescence spectra of fractions from vessel III. **d** Digital camera images of composite strips made from CdSe NPs with different sizes, recorded under UV irradiation at 365 nm (size: 105 mm × 20 mm)

6.3 Synthetic Optimization Through DGUC Nanoseparation

The crystallization behaviors of inorganic nanostructures are often different even in one-pot synthesis since the microenvironment of their nucleation and growth cannot be exactly the same. Synthetic optimization is therefore usually hard to be performed by traditional contrast experiments. In view of the fact that nanoparticles with different size, morphology, or phase can be separated through DGUC nanoseparation, by analyzing the chemical composition or crystal structure of separated fractions, key pieces of information can be obtained and thus guide synthetic optimization [11].

Cadmium sulfide (CdS) semiconducting nanorods (NRs), known as quantum rods, have attracted an enormous amount of attention due to their promising applications. Although extensive effort has been devoted to control the anisotropic growth of CdS NRs, more effective methods should be developed to regulate the nucleation and growth processes to obtain CdS nanorods with precisely tailored electrical and optical properties [12].

Inspired by nanoseparation, in 2011, Sun's group have performed the separation of CdS NRs [13]. After centrifugation in a cyclohexane + tetrachloromethane gradient at 30000 rpm for 135 min, longer CdS NRs could be observed at lower positions of the centrifuge tube, as shown in Fig. 6.6, which suggested that the weight of a NR played the dominant role on its sedimentation rate.

HRTEM images of CdS NR in corresponding fractions in Fig. 6.7a further confirmed the length evolution. Besides, the photoluminescence spectra in Fig. 6.7b showed a blueshifted band-edge emission. The relationship between the length of

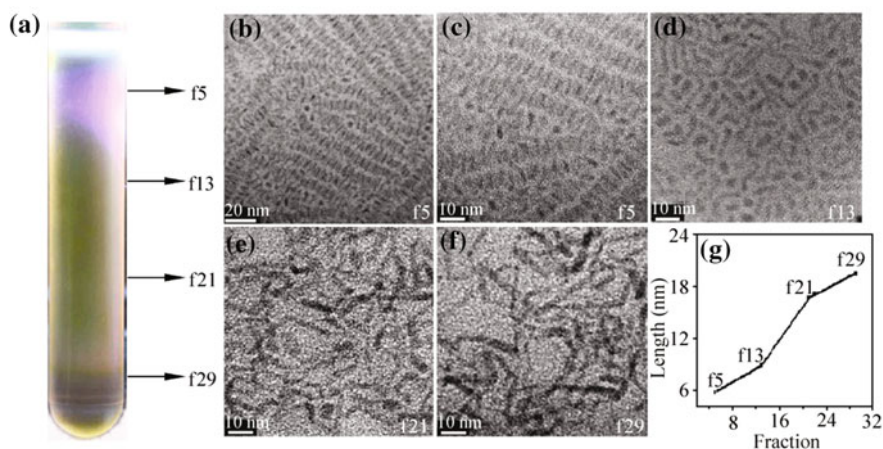


Fig. 6.6 **a** Digital camera images of ultracentrifuge tubes containing CdS NRs after separation, recorded under irradiation at 365 nm. **b–f** TEM images of corresponding CdS NR fractions. **g** Length evolution of CdS NRs in different fractions

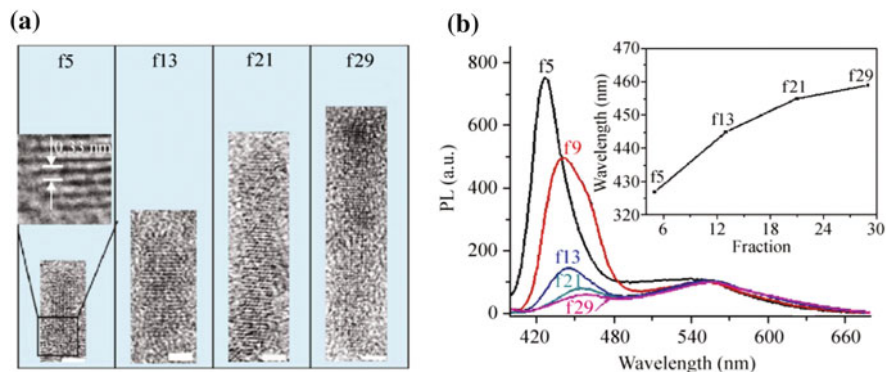


Fig. 6.7 **a** Typical HRTEM images and **b** photoluminescence spectra of CdS NRs fractions (scale bar: 2 nm, the inset presents a plot of the band-edge emission peak positions of corresponding fractions)

CdS NRs and their photoluminescence properties became apparent after separation, which inspired them to selectively prepared monodisperse samples by synthetic optimization.

As reported by Papadimitrakopoulos, the presence of oxygen can promote the transformation of CdSe quantum dots to nanorods. Here, CdS nanorods were synthesized in N_2 , air, and O_2 atmosphere, respectively. As expected, N–CdS contained the shortest nanorods with photoluminescence dominated by short wavelength band-edge emission while O–CdS NRs were the longest and long wavelength surface-trap emission predominated (Fig. 6.7). This indicated that oxygen-deficient condition could lead to the formation of ultrashort CdS nanorods, which were nearly the same as that obtained in f5 after separation of A–CdS (Fig. 6.8).

In 2013, Sun's group also studied the phase transition of Yb^{3+} and Er^{3+} co-doped $NaYF_4$ nanocrystals ($NaYF_4:Yb^{3+}/Er^{3+}$ NCs) using density gradient ultracentrifuge separation [14]. The $NaYF_4:Yb^{3+}/Er^{3+}$ NCs were synthesized in an oleic acid–water–ethanol system via hydrothermal process. After separation, the fraction 1 was orange colored under excitation at 980 nm, and the middle fraction 6 turned red while fraction 18 at the bottom exhibited green emissions, as shown in Fig. 6.9.

The structural and compositional difference among these three fractions was investigated using transmission electron microscopy. f1 and f14 were composed of ~ 28 and ~ 44 nm nanocubes, respectively, meanwhile, f18 was composed of ~ 1.2 μm nanorods. It was found that f1 and f14 had relatively high Y atomic ratio and f18 was richer in Yb and Er.

The size, morphology and composition difference inspired Sun's group to verify the sharp and composition evolution by monitoring the formation process by TEM and EDS at different reaction time points (Fig. 6.10). When the reaction lasted for

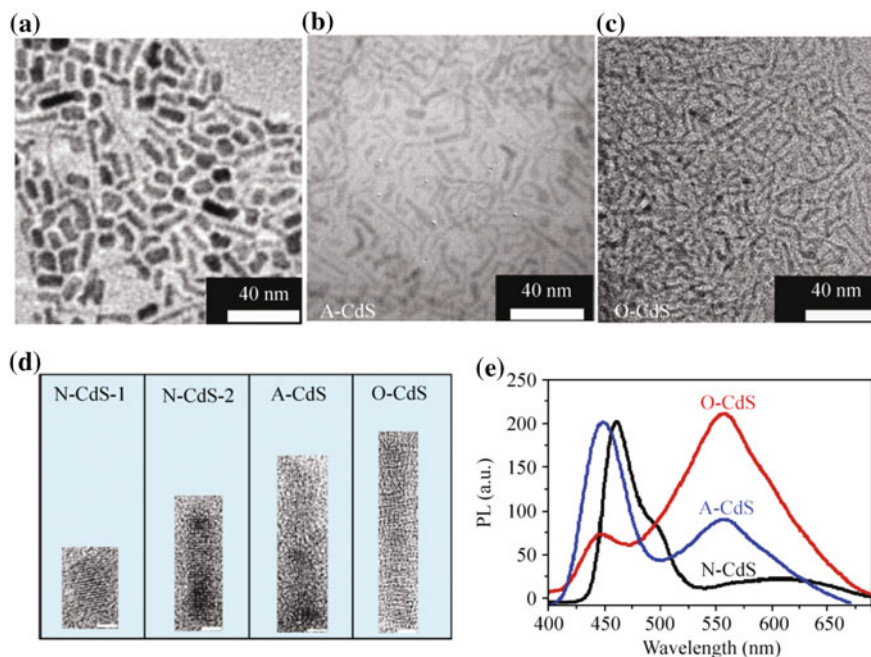


Fig. 6.8 a–c TEM images of CdS NRs prepared in N_2 (N–CdS), air (A–CdS), and O_2 (O–CdS), respectively. **d** Typical HRTEM images and **e** photoluminescence spectra of corresponding CdS NRs (there are two kinds of rods in N–CdS, which are denoted as “N–CdS-1” and “N–CdS-2”)

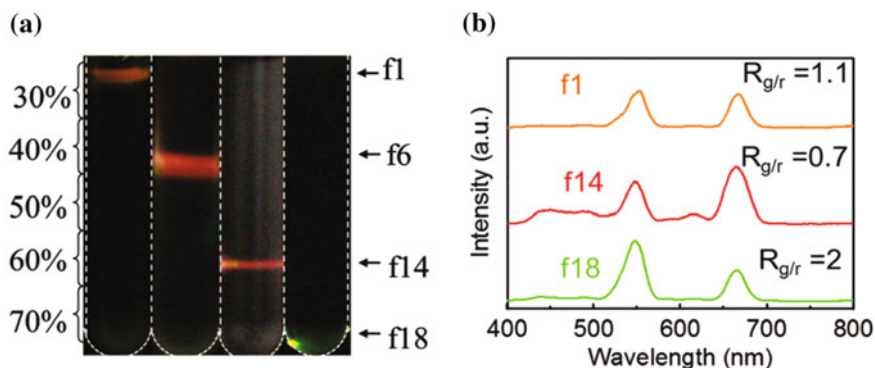


Fig. 6.9 a Digital camera images of ultracentrifuge tubes containing $NaYF_4:Yb^{3+}/Er^{3+}$ NCs after separation under excitation at 980 nm; **b** UC fluorescence spectra of typical $NaYF_4:Yb^{3+}/Er^{3+}$ NCs fractions

1.5 h, pure α -phase $NaYF_4:Yb^{3+}/Er^{3+}$ nanocubes were obtained and the Y:Yb:Er atomic ratio was found to be 83:16:1, which was nearly the same as f1. As the reaction time was prolonged to 20 h, mixed phases were appeared, indicating a

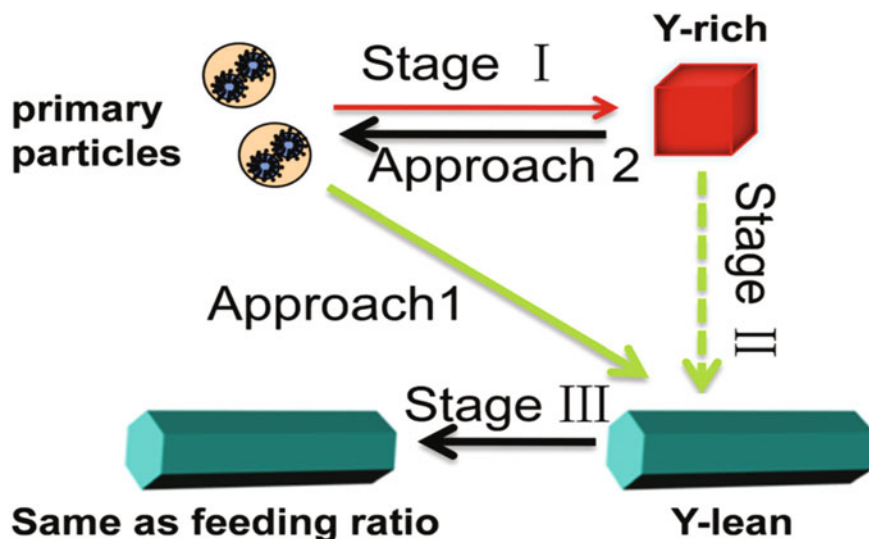


Fig. 6.10 Schematic illustration of the formation process of NaYF₄:Yb³⁺/Er³⁺ NCs

phase transition. At last, when the reaction lasted for 7 days, the atomic ratio of Y:Yb:Er returned to 78:20:2, which was the same as the feeding ratio. Thus, a plausible mechanism of morphological and compositional evolution was proposed. Namely, small cubes (f1) with a higher Y content were formed at the initial stage, the subsequent phase transition (stage II) led to the formation of thermally stable β -phase nanorods, which were rich in Yb. After the dissolution–crystallization equilibrium (stage III), the Y:Yb:Er atomic ratio turned the same as the feeding ratio, and the nanorods became bigger in size.

6.4 Surface Reaction Mechanism Investigation Through “Reaction Zone” in the Density Gradient

To date, the investigation on surface reaction mechanism still critically relies on the capture of reaction intermediates [15–17]. However, high surface area of NPs endows NPs with high reactivity, which lead to a quick reaction rate, but unfortunately, such intermediates are usually hard to be obtained in a short time through traditional centrifugation methods.

DGUC nanoseparation method provides new opportunity of isolating intermediate NPs within a short period of time. By introducing a reaction zone in gradient layers, surface reaction mechanism can be investigated, since the reaction time can be finely controlled and the chemical environment can be changed very soon.

As an example, to investigate the surface reaction mechanism of galvanic replacement reaction between Au and Ag, a 20% to 70% EG/H₂O gradient layers

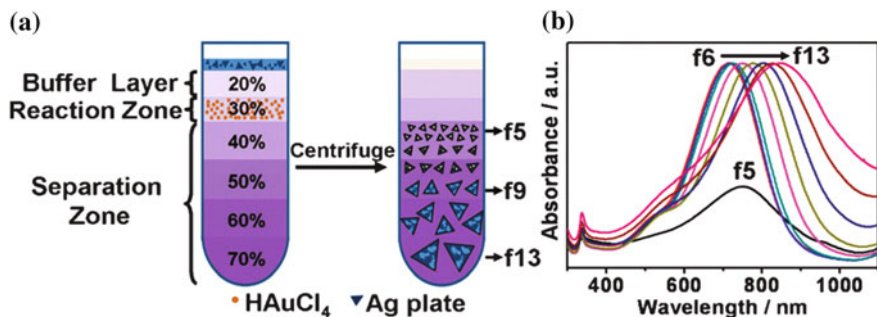


Fig. 6.11 **a** Schematic illustration of surface reaction mechanism investigation through DGUC nanoseparation by introducing a reaction zone. **b** UV-Vis spectroscopy of the corresponding fractions

were used in centrifugation [4]. As shown in Fig. 6.11 a, the second layer was set as reaction zone by introducing a certain amount of reactant “HAuCl₄” and the first layer was used as a buffer layer to prevent a direct mixing and reaction. Furthermore, the lower four layers acted as the separation zone to separate the reacted Ag nanoplates by their sizes. Ag nanoplates prepared in aqueous phase was placed on the top of the gradient layers. As shown in Fig. 6.11 b, after separation, a clearly redshifting could be observed, demonstrating the increased size of reacted Ag nanoplates from f6 to f13. However, f5 did not show the similar trend, which should be attributed to the hollow structures.

The hollow structure of Ag nanoplates in f5 was further confirmed by TEM, as shown in Fig. 6.11a. Ag nanoplates with smaller size should have slower sedimentation rate, which could lead to a longer exposure time and thus result in their hollow structures. On the contrary, bigger Ag nanoplates should have a shorter exposure time, which should result in a short-time reaction. As estimated, the exposure time of f9 in reaction zone was only 30 ± 17 s, which is much shorter than that can be achieved by traditional reaction and centrifugal process.

To get deeper insight into the surface reaction mechanism, the Ag nanoplates in f9 were characterized by HRTEM and EDS. The Au/Ag atomic ratio of the edge regions was measured to be 0.231, much higher than other regions, indicating the edge side should be the favored site for such surface reaction. Besides, the Au/Ag atomic ratio of thick and thin part of the basal plane was 0.064 and 0, respectively. This means the thin part presents the Ag dissolution zone and the thick part should be responsible for the Au deposition.

On the basis of the results above, the structural evolution of triangular Ag nanoplates during the surface reaction can be divided into two stages, as shown in Fig. 6.12c. At the initial stage, the reaction starts at the edge side and at the same time on the basal plane surface. With the reaction time increasing, Ag dissolution and Au deposition jointly lead to the formation of hollow structure when the reaction comes to its end at stage II.

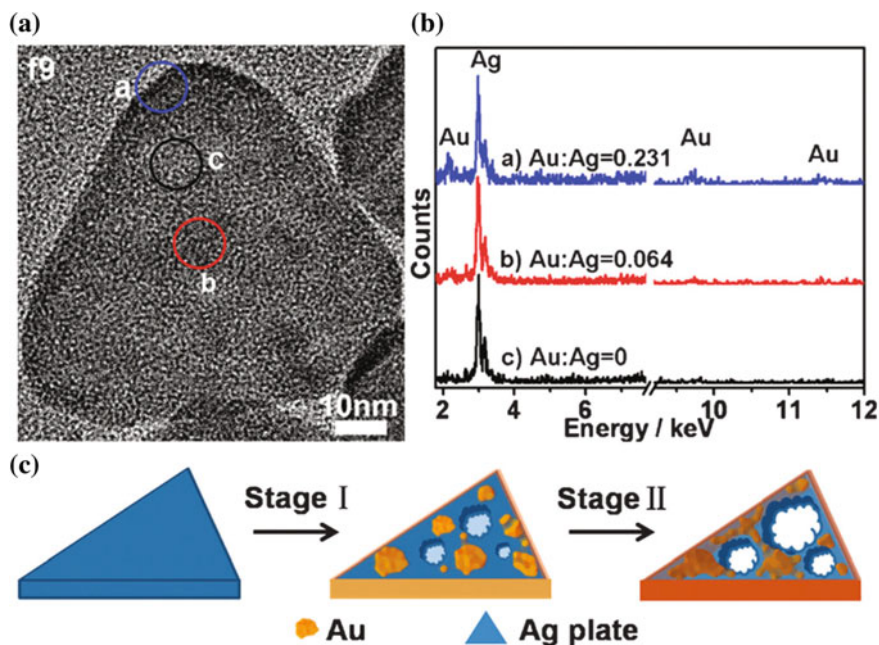


Fig. 6.12 **A** HRTEM image of typical reacted Ag nanoplate in f9 and **B** the EDS results of corresponding regions as marked in the HRTEM image: **a** edge; **b** thick part and **c** thin part of the basal plane. **C** Schematic illustration of the structural evolution of a triangular Ag nanoplate during the surface reaction

6.5 Controlled Asymmetric Assembly Through “Assembly Zone” in the Density Gradient

Controlled assembly of NPs is critical for the investigation on their collective properties, which is of great importance in guiding the fabrication of elaborate nanodevices [18, 19]. However, currently, random Brownian motions remained the only way to achieve the asymmetric assembly of NPs and such uncontrollable method has greatly limited the application of the assembly structures. Since centrifugal field can be applied to overcome the Brownian motion effect of NPs, DGUC separation can be designed to make colloidal heteroassembly by introducing an “assembly zone” in the density gradient layers [20].

During the centrifugal process, the directional motion of bigger NPs should be faster than that of NPs with smaller size and thus symmetric heteroassemblies can be fabricated by a “crash reaction” as schematically shown in Fig. 6.13a. Big Au NPs, ~ 60 nm in diameter and with a positively charged surface, were placed on the top of the density gradient layers. Meanwhile, ~ 20 nm Au NPs with a negatively charged surface were set at a lower layer, with a buffer layer inserted to avoid a spontaneous assembly. When a large centrifugal force was applied, big Au NPs

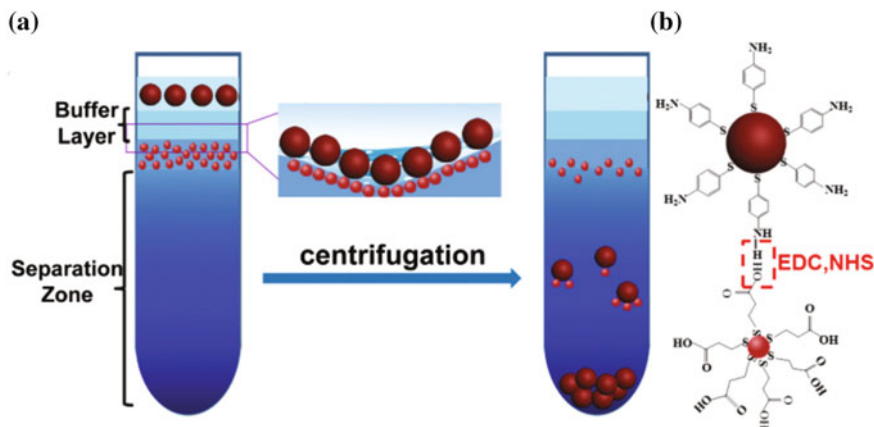


Fig. 6.13 **a** Schematic illustration of controlled asymmetric assembly of different sized Au NPs through “crash reaction” in density gradient centrifugation. **b** Schematic linkage of functionalized Au NPs through dehydration condensation reaction

can cross through the buffer layer and react with small ones with opposite charge (Fig. 6.13b) [21].

Figure 6.14 shows a typical result of asymmetric assembly in the density gradient. After the “crash reaction,” the UV–Vis spectra showed a slight redshift from f18 to f22 (Fig. 6.14b), demonstrating the successful assembly of Au NPs. Besides, TEM images in Fig. 6.14c, d further confirmed the asymmetric assembly. However, it should be noted that the assembling efficiency was not high enough, resulting in only a small portion of effective collision.

6.6 Ultraconcentration of Colloidal NPs Through Water/Oil Interfaces

As a high-efficiency separation and purification way density gradient centrifugation can avoid colloidal nanoparticles from nanostructure destruction and aggregation. This separation is appropriate to aqueous phase or organic phase. However, what will happen as the nanostructures passing through oil–water interface in the centrifuge tube during centrifugation? Kuang et al. had a detailed study in this aspect. Density gradient centrifugation of colloidal NPs through water/oil interface becomes a high-efficiency way to achieve NPs purification and concentration without any aggregation [22]. The interface between different layers of density gradient concentrate the nanoparticles while separation progress. NPs will pass through the interface after the enrichment (Fig. 6.15a). For certain nanoparticles, small droplet could be formed under high centrifugal force which leads fast

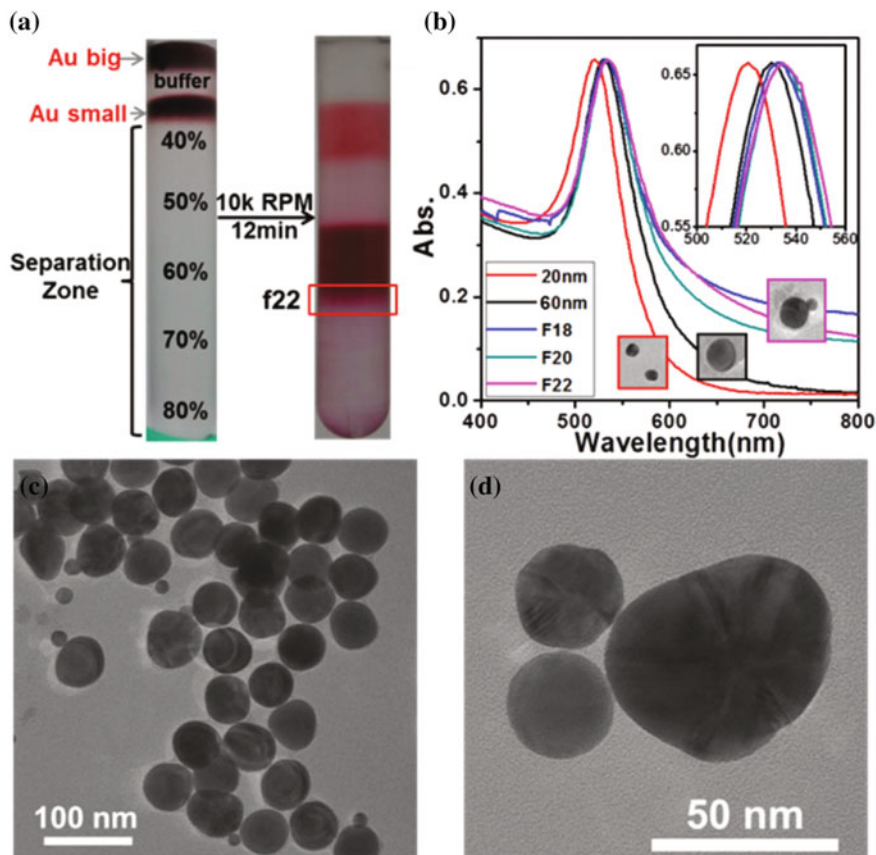


Fig. 6.14 **a** Digital camera images of the density gradient layers before and after "crash reaction" in centrifugation. **b** UV-Vis spectra of corresponding fractions after separation. **c** and **d** TEM images of the Au NP assemblies in f22

sedimentation, while larger droplet formed under low centrifugal force which needs more time to accumulate at interface.

Ultraconcentration of colloidal NPs through water/oil interfaces apply to zero-dimensional nanoparticles, one-dimensional nanomaterials, and two-dimensional nanosheets. While some low-density nanosheets can't pass through water/oil interface, such as graphene and graphene oxide because centrifugal force is not enough to overcome buoyancy force and interfacial tension, thus graphene oxide will concentrate at the interface.

The volume of bottom ultraconcentration colloidal NPs was too small to measure, spectroscopy linear curve fitting method was used to test volume and concentration while diluting. In order to ensure the measurement is accurate, it is necessary to use organic liquid seal keep the ultraconcentration volume same. In order to make sure that density of 30% CCl_4 /cyclohexane liquid seal is lower than

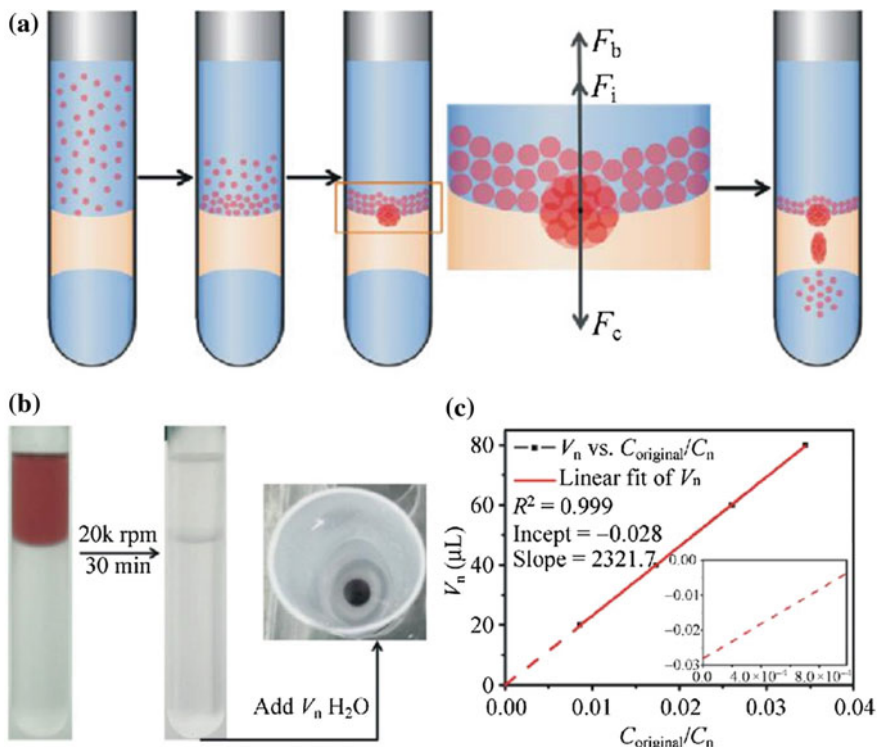


Fig. 6.15 **a** Schematic illustration of droplet sedimentation. **b** Gradient centrifugation in centrifuge tube with minimized the volume of bottom layer. **c** Graph between V_n and $C_{original}/C_n$

water, add cyclohexane to the organic layer so the water won't float on the organic layer when diluting the ultraconcentration colloidal NPs.

$$C_n(V_n + V_0) = C_0V_0$$

Volume and concentration of ultraconcentration colloidal NPs assume as V_0 and C_0 , respectively. Add volume water V_n to dilute the colloidal solution concentration to C_n . Based on the Beer–Lambert law, C_n could be calculated by UV–Vis spectroscopy. Liquid seal has ensured the V_0 stay the same during the dilution. In this premise, the concentration of original Au nanoparticle assumes as $C_{original}$ that the formula transformed into $V_n = C_0V_0/C_n - V_0 = (C_0/C_{original}) V_0/(C_n/C_{original}) - V_0$. Therefore, after calculation of the $C_0/C_{original}$ by Beer–Lambert law, a linear plot with intercept $-V_0$ and slope equal to $(C_0/C_{original}) V_0$ can be obtained. By fitting the slope and intercept, ultraconcentration solution volume and relative increased multiples to the original solution can be calculated.

After calculation, 3 ml Au colloidal NPs pass through water/oil interface was concentrated to 0.028 μ l and the concentration increased at least 10^4 times. In such

high concentration, the density of ultraconcentration solution up to 5.28 g/ml and the packing density of Au NPs up to 64.2% which is close to the limit of closely packed packing density (74%). Herein, the ultraconcentration Au colloidal NPs were staying in the closely packed state which almost presented a solid state. Under such high packing density, the colloid NPs still without aggregation and maximize the dispersed state. Such a high-efficient concentration proves that the water/oil interface centrifugation method is very efficient on purification. The research mentioned above 64.2% volume of ultraconcentration colloid was occupied by Au NPs. So there was only 0.01 μl original solution pass through the water/oil interface which means the purification way could remove the 99.99% impurity one-time only. Such high-efficient way demonstrates superiority than other separation methods.

References

1. Duan R, Zuo X, Wang S et al (2013) Lab in a tube: ultrasensitive detection of microRNAs at the single-cell level and in breast cancer patients using quadratic isothermal amplification. *J Am Chem Soc* 135(12):4604–4607
2. Smith EJ, Schulze S, Kiravittaya S et al (2010) Lab-in-a-tube: detection of individual mouse cells for analysis in flexible split-wall microtube resonator sensors. *Nano Lett* 11(10):4037–4042
3. Harazim SM, Quiñones VAB, Kiravittaya S et al (2012) Lab-in-a-tube: on-chip integration of glass optofluidic ring resonators for label-free sensing applications. *Lab Chip* 12(15):2649–2655
4. Zhang C, Luo L, Luo J et al (2012) A process-analysis microsystem based on density gradient centrifugation and its application in the study of the galvanic replacement mechanism of Ag nanoplates with HAuCl₄. *Chem Commun* 48(58):7241–7243
5. Liu C, Fan Y, Liu M et al (1999) Hydrogen storage in single-walled carbon nanotubes at room temperature. *Science* 286(5442):1127–1129
6. Odom TW, Huang J-L, Kim P et al (1998) Atomic structure and electronic properties of single-walled carbon nanotubes. *Nature* 391(6662):62–64
7. Bachilo SM, Strano MS, Kittrell C et al (2002) Structure-assigned optical spectra of single-walled carbon nanotubes. *Science* 298(5602):2361–2366
8. Sun X, Zaric S, Daranciang D et al (2008) Optical properties of ultrashort semiconducting single-walled carbon nanotube capsules down to sub-10 nm. *J Am Chem Soc* 130(20):6551–6555
9. Murray C, Norris DJ, Bawendi MG (1993) Synthesis and characterization of nearly monodisperse CdE (E = sulfur, selenium, tellurium) semiconductor nanocrystallites. *J Am Chem Soc* 115(19):8706–8715
10. Bai L, Ma X, Liu J, Sun X et al (2010) Rapid separation and purification of nanoparticles in organic density gradients. *J Am Chem Soc* 132(7):2333–2337
11. Ma X, Kuang Y, Bai L et al (2011) Experimental and mathematical modeling studies of the separation of zinc blende and wurtzite phases of CdS nanorods by density gradient ultracentrifugation. *ACS Nano* 5(4):3242–3249
12. Zhang G, He P, Ma X et al (2012) Understanding the “Tailoring Synthesis” of CdS nanorods by O₂. *Inorg Chem* 51(3):1302–1308
13. Sun X, Ma X, Bai L et al (2011) Nanoseparation-inspired manipulation of the synthesis of CdS nanorods. *Nano Res* 4(2):226–232

14. Song S, Kuang Y, Liu J et al (2013) Separation and phase transition investigation of Yb³⁺/Er³⁺ + co-doped NaYF₄ nanoparticles. *Dalton T* 42(37):13315–13318
15. Chatterjee D, Deutschmann O, Warnatz J (2002) Detailed surface reaction mechanism in a three-way catalyst. *Faraday Discuss* 119:371–384
16. Long R, Yang R (2002) Reaction mechanism of selective catalytic reduction of NO with NH₃ over Fe–ZSM-5 catalyst. *J Catal* 207(2):224–231
17. Koop J, Deutschmann O (2009) Detailed surface reaction mechanism for Pt-catalyzed abatement of automotive exhaust gases. *Appl Catal B Environ* 91(1):47–58
18. Chen G, Wang Y, Yang M et al (2010) Measuring ensemble-averaged surface-enhanced Raman scattering in the hotspots of colloidal nanoparticle dimers and trimers. *J Am Chem Soc* 132(11):3644–3645
19. Urban AS, Shen X, Wang Y et al (2013) Three-dimensional plasmonic nanoclusters. *Nano Lett* 13(9):4399–4403
20. Qi X, Li M, Kuang Y et al (2015) Controllable assembly and separation of colloidal nanoparticles through a one-tube synthesis based on density gradient centrifugation. *Chem Eur J* 21(19):7211–7216
21. Song S, Kuang Y, Luo L et al (2014) Asymmetric hetero-assembly of colloidal nanoparticles through “crash reaction” in a centrifugal field. *Dalton Trans* 43(16):5994–5997
22. Kuang Y, Song S, Liu X et al (2014) Solvent switching and purification of colloidal nanoparticles through water/oil Interfaces within a density gradient. *Nano Res* 7(11):1670–1679